Journal of Materials Research and Technology 41 (2026) 1814–1826

Contents lists available at ScienceDirect

Journal of Materials Research and Technology

journal homepage: www.elsevier.com/locate/jmrt

Insights into the microstructure evolution and micromechanical properties of friction stir consolidated AA6082 aluminum chips

S. Emami [a], G. Buffa [a,*], A. Latif [a], Giulia Stornelli [b], Andrea Di Schino [b], B. Särnerblom [c], V. Patel [c], L. Fratini [a]

[a] Department of Engineering, University of Palermo, Viale delle Scienze, Palermo, 90128, Italy
[b] Department of Engineering, University of Perugia, Via G. Duranti 93, 06125, Perugia, Italy
[c] Department of Engineering Science, University West, Trollhättan, 46186, Sweden

ARTICLE INFO

Keywords:
Friction stir consolidation
Microstructure
Grain size
CDRX
Texture

ABSTRACT

Friction stir consolidation (FSC) is a relatively new solid-state recycling process developed to obtain small billets from metal chips in a unique working step. One of the main unresolved issues in solid-state recycling processes (e.g., Friction Stir Extrusion, Continuous Friction Extrusion, etc.) is the understanding of the effects of the oxide layers initially present on the chips on the final recycled products. In this paper, FSC was conducted on AA 6082 aluminum chips with different rotational speeds of 1000, 1500, 2000, and 2500 rpm. Microstructural evolution was examined using scanning electron microscopy (SEM) integrated with electron backscattered diffraction (EBSD). Backscattered electron (BSE) images showed that fine equiaxed grain structures were developed through the microstructure of the processed samples. Intermetallic compounds were broken down by the stirring action of the rotating tool, leading to the formation of micro- and nano-sized second-phase particles. The presence of loose high-angle grain boundaries connected to low-angle grain boundaries confirmed the occurrence of continuous dynamic recrystallization (CDRX). Texture analysis revealed the development of simple shear texture components of face-centered cubic (FCC) structured materials with the Oblique Cube component. Hardness measurements revealed that the hardness of the microstructure increased with a greater proportion of low-angle grain boundaries (LAGBs) and higher texture intensity.

1. Introduction

In the last few years, recycling techniques of metallic scraps have gained the attention of academia and industry as they provide relevant economic and environmental benefits. The melting-based traditional approach is potentially associated with inherent problems such as higher metal loss attributed to the higher chemical reactivity, higher energy consumption, and finished costs. On the other hand, solid-state techniques eliminate the problems associated with melting and effectively reduce the contamination and the cost of recycling [1]. Researchers have conducted some investigations on the recycling of materials with solid-state techniques, which have mainly focused on the feasibility of the considered technique. Güley et al. [2] conducted a study on the solid-state recycling of AA6060 chips using hot extrusion. The authors stated that breaking the oxide layers is a precondition for chip welding and provided a criterion for their sound bonding. Mohammed et al. [3] examined the influence of the ECAP process on the mechanical properties and microstructure of recycled AA-6061 chips. Their investigation mainly focused on the mechanical properties of the introduced materials and microstructure characterization using optical micrographs. Al-Alimi et al. [4] investigated solid-state recycling of AA6061 chips reinforced with B_4C particles by hot extrusion followed by hot ECAP. Selmy et al. [5] investigated the solid-state recycling of aluminum alloy (AA-6061) chips through a two-step process involving hot extrusion followed by equal channel angular pressing (ECAP) at room temperature. Their findings demonstrated that elevated extrusion temperatures, coupled with intensified plastic deformation during the ECAP process, significantly enhanced interfacial bonding between the consolidated chips. They reported the presence of boundaries as barriers against grain growth and investigated the impact of different passes of ECAP on grain size distribution. Taha et al. [6] conducted an investigation into the corrosion behavior of recycled AA6061 aluminum chips processed via hot extrusion followed by ECAP. Abd El Aal [7] recycled Al chips and Al chips composites using high-pressure torsion (HPT). The

* Corresponding author.
E-mail address: gianluca.buffa@unipa.it (G. Buffa).

https://doi.org/10.1016/j.jmrt.2026.01.001
Received 2 July 2025; Received in revised form 16 December 2025; Accepted 2 January 2026
Available online 2 January 2026

author reported that high-pressure torsion (HPT) applied to aluminum powders and chips produced microstructures with finer grain sizes and a higher fraction of high-angle grain boundaries (HAGBs) compared to those obtained from HPT-processed solid samples. The formation of a refined microstructure with a high fraction of high-angle grain boundaries (HAGBs) was attributed to the presence of oxide layers on the surfaces of the processed aluminum powders and chips. It was also found that the HPT produces ultrafine-grained (UFG) recycled bulk aluminum chips and chip composites exhibiting a trimodal microstructure (a mixture of micro, UFG, and Nano grain sizes). This structural heterogeneity was attributed to variations in dislocation density and the non-uniform plastic deformation. Shi et al. [8] explored the influence of processing parameters on the relative density, microhardness, and microstructure of recycled Ti–6Al–4V alloy, fabricated from machining chips through the ECAP. They showed that the chips aligned themselves in the direction of the applied shear, the bonding between the chips improved with increasing the number of the ECAP passes and the lamellar structure was replaced by equiaxed grains at a higher number of passes. Haase et al. [9] employed an integrated extrusion and equal channel angular pressing (iECAP) technique to recycle AA6060 aluminum chips. They used optical microscopy to show different microstructural regions and material flow patterns created during the processing. Whalen et al. [10] employed EBSD to characterize the microstructure of recycled AA6063 aluminum industrial scrap processed through shear-assisted processing and extrusion. They used inverse pole figure maps to show the introduced microstructure and used pole figures to show the generated texture of the recycled material in different regions. Kolpak et al. [11] developed a welding model to numerically predict the feasibility of aluminum chip extrusion and conducted hot extrusion experiments to determine a weld quality factor that ensures successful processing without local delamination. Chiba et al. [12] investigated the feasibility of the solid-state recycling of aluminum alloy machining swarf into c-channels using hot extrusion. Tao et al. [13] investigated the recycling of AZ91 Mg alloy machining chips by extrusion and ECAP. They attributed the improvement of the tensile properties to fine grain structure and dispersed oxide contaminants. Pei et al. [14] conducted a systematic study on the recovery of homogenized Mg-Gd-Y-Zn-Zr alloy chips through isothermal sintering and ECAP.

Recently, researchers have focused on the possibility of using Friction Stir Consolidation (FSC) to recycle the machining chips [15–19]. Ingarao et al. [15] conducted a life cycle assessment of aluminum recycling using both single-step and multi-step FSC processes. Li et al. [16] employed FSC to transform AA6061 aluminum machining chips into solid discs. The results showed the presence of a banded structure similar to onion rings which is attributed to the flow patterns caused by a thermo-mechanical cycle during processing. They reported the presence of a dead zone at the bottom of the billet which never experienced deformation even at prolonged deformations. Buffa et al. [17] studied the feasibility of the FSC process as aluminum chips recycling process. They identified a direct correlation between the mass of aluminum chips undergoing consolidation and the amount of heat generated during the FSC process, which is provided by the tool rotational speed and the dwelling time. They demonstrated that an improper balance between chip mass and heat input during FSC leads to microstructural defects, such as void formation. Latif et al. [18] applied the FSC process to fabricate functionally graded billets from a combination of AA7075 and AA2011 aluminum alloy chips, enabling the production of multi-material structures. In another study [19], To address issues inherent in single-step FSC—such as unconsolidated chips at the billet base and non-uniform mechanical properties—these researchers implemented a double-sided approach, enhancing consolidation quality and property uniformity across the billet. Their findings confirmed that the two-step FSC process achieved full billet consolidation and significantly enhanced the mechanical properties. Behnagh et al. [20] employed a double-step FSC process to explore the feasibility of fabricating seamless tubes from aluminum machining chips. The results revealed the presence of dynamically recrystallized grains throughout the microstructure of the fabricated tube. Abebe et al. [21] conducted a systematic investigation to optimize the wear performance of metal matrix hybrid composites produced via the FSC process. The results showed that the optimal wear rate of 0.008 mg/m was achieved with a sliding distance of 350 m, a sliding speed of 240 rpm, and a load of 20 N. Latif et al. [22] examined the forgeability of billets consolidated from dissimilar aluminum alloy chips—AA7075 and AA2011-T3—in both mono-material and bi-material configurations. They reported that forging and upsetting significantly enhanced the hardness of the FSCed billets. Cracks in the form of surface debonding were observed during the upsetting of mono-material billets, particularly in the case of the low-ductility aluminum alloy AA7075. It is well known that during hot working, dynamic restoration phenomena such as dynamic recovery and recrystallization determine the final microstructure and properties of the evolved material. Moreover, the presence of oxides and second-phase particles can effectively influence the final mechanical properties of the materials [23,24] as their presence is inevitable in the microstructure of the recycled materials with solid-state techniques.

The survey of the literature reveals that studies have mainly focused on the feasibility of the different solid-state techniques in recycling machining chips and their mechanical assessment. Microstructural evolution and the evolution of the constituent oxide layers (which remain in the alloy and can deteriorate the final properties of the recycled material [25]) during the FSC process has not been investigated yet. This study investigates the influence of processing parameters on grain structure and substructural evolution, as well as the redistribution of constituent oxide layers during the recycling of AA6082 aluminum chips via FSC, utilizing advanced characterization techniques of scanning electron microscopy (SEM) and electron backscatter diffraction (EBSD).

2. Materials and methods

The starting material was an extruded square bar of aluminum alloy AA 6082 with a cross-sectional area of 30 mm by 30 mm. The considered alloy was selected due to its widespread use in the transport industry. Particularly, the automotive sector is one of the major sources of aluminum scraps [26], and therefore, it is extremely important to recycle these discarded products for efficient energy and resource utilization. The squared bar of AA 6082 was reduced into chips through a milling operation with details listed in Table 1.

This technique utilizes frictional and deformational heat to soften the material and vertical pressure provided by a non-consumable tool to join and consolidate the severely deformed chips. To ensure effective cleaning, the aluminum chips were submerged in acetone for 30 min. A 15 g batch of chips was then loaded into a cylindrical die with a nominal diameter of 25.4 mm and compacted using a 25 mm diameter H13 steel tool under a force of 5 kN. Compaction was performed to prevent chip displacement during the subsequent FSC process.

The die and pressing tool system was assembled with the working table and head of ESAB-LEGIO (Fig. 1), a dedicated friction stir welding machine. Then Tool rotation was initiated under an initial pressing load of 5 kN. This load was then linearly increased at a rate of 0.5 kN/s to reach the target values of 10, 15, or 20 kN. This gradual increase, referred to as the transition phase, was necessary due to machine

Table 1
Process conditions of milling operation for producing AA 6082 chips.

Operation	Tool	Number of teeth	Rotational speed [RPM]	Feed rate [mm/min]	Depth of cut [mm]
Milling	BDMT11T308ER-JT PR1225	3	1250	280	1

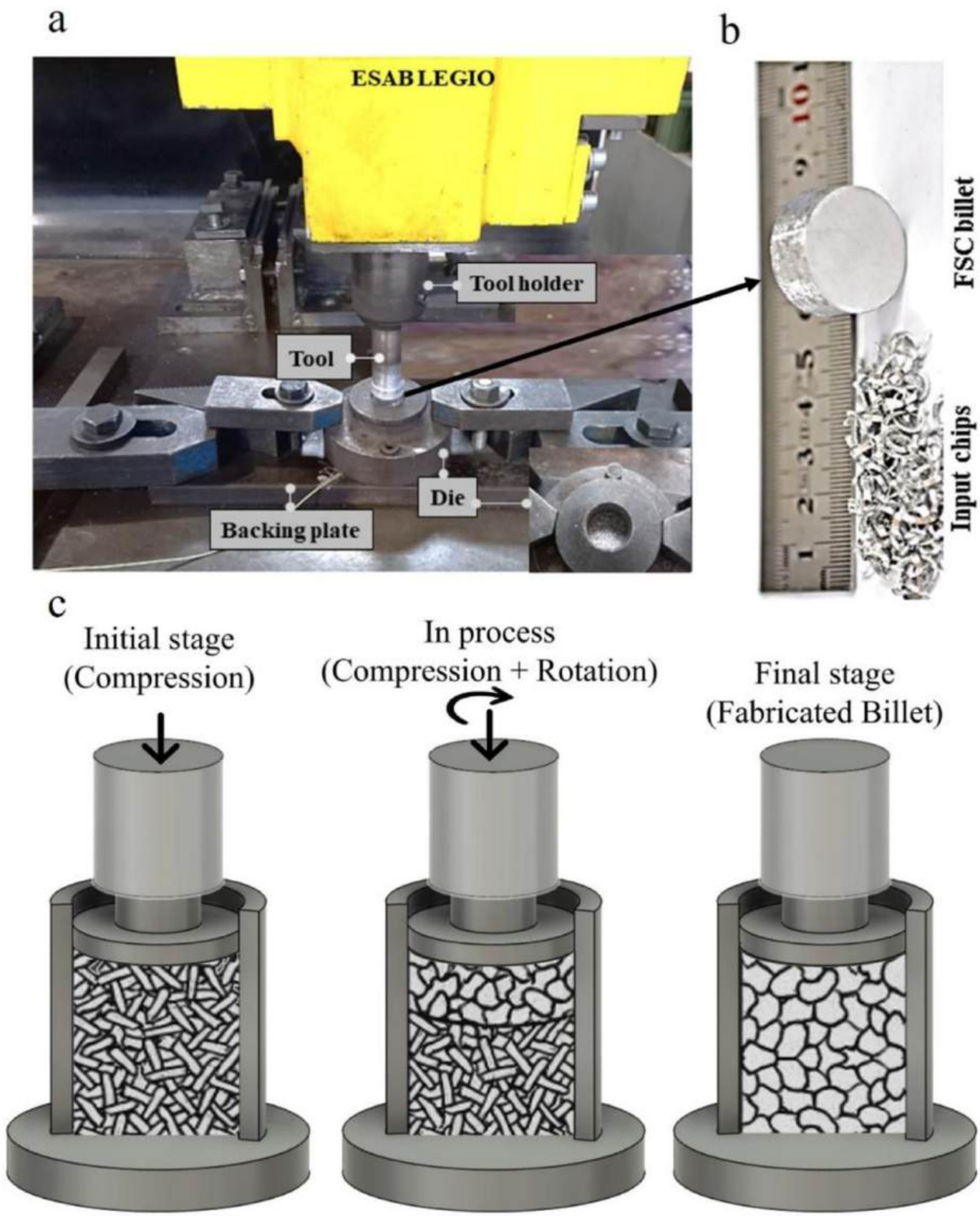

Fig. 1. Friction stir consolidation: a) experimental setup, b) input chips with consolidated billet, and c) process schematic showing the steps of billet fabrication.

limitations that prevented an instantaneous jump from 5 kN to the desired load. Upon reaching the desired load, the time during which the billet was consolidated was referred to as consolidated time. The total processing time comprised the transition and consolidation phases. Cylindrical billets were manufactured from chips at different rotational speeds, consolidation forces, and various processing times in accordance with the experimental plan outlined in Table 2.

Manufactured FSC billets were first sectioned and then polished using a series of abrasive papers. At the final stage of polishing, alumina was applied as a polishing lubricant. Microstructure was revealed by applying Keller's Weck reagent [1 g NaOH, 4g KMnO4, and 100 ml H2O], and the microstructure was analyzed across different zones of the FSC billet using SEM. The scanning electron microscopy samples were subjected to multistep grinding and mechanical polishing using 3 μm diamond suspension, which was subsequently followed by polishing with colloidal silica. Scanning electron microscopy analyses were conducted using a Zeiss field emission scanning electron microscope, equipped with symmetry electron backscatter diffraction (EBSD) and Oxford energy dispersive spectroscopy (EDS) detectors. The results obtained were analyzed using ATEX software version 4.14 [27]. EBSD data were obtained from a longitudinal cross-section parallel to the vertical downforce. EBSD specimens were mechanically pre-polished with 1 and 50 nm alumina suspension.

3. Results and discussion

Figs. 2 and 3 represent the microstructures obtained from different regions, i.e., A, B, C, and D, of samples processed with different parameters. It is visible for all the parameters that there is no trace of layer bonding, which shows the effectiveness of the parameters on the consolidation of the materials. Against other solid-state techniques like ECAP, through which the bonding between the chips takes place with a layered morphology, friction stir-related processes can effectively stir the material and remove the initial microstructure [28].

It can be seen from the figures that equiaxed grains have been formed during the process through the microstructure of the evolved materials for all the considered parameters. The co-existence of higher degrees of temperature and deformation encourages the occurrence of thermally activated phenomena, such as recovery and recrystallization, through the microstructures which result in the development of fine equiaxed grains [28]. Grain refinement is one of the desirable modifications that usually take place during hot deformation processes [23], such as shear-assisted processing and extrusion of 6063 [29] and 7075 [30] aluminum alloys, and friction extrusion of AA7075 Al alloy [31]. Fig. 4 shows the average grain size distribution for the four different zones of the specimens previously identified, as a function of the considered process parameters, i.e., tool rotation, tool force, and processing time. Grain size measurements showed that, at a fixed vertical downforce and processing time, a larger grain size is obtained for higher rotational speeds as the generated heat increases with rotational speed (Fig. 3).

The results also revealed that the grain size increases with the vertical downforce at a given rotational speed and processing time. The same trend was observed with increasing processing time at a fixed rotational speed and vertical downforce. Microstructures show that from the regions near the shoulder (A and C) towards the bottom of the billets (B and D), the grain size tends to decrease in almost all the manufactured billets. This behavior indicates that temperature is the dominant factor and results in a coarse-grained structure. It is well accepted that different processing parameters provide the material with different amounts of deformation and different temperatures, which, in turn, determine the final microstructure of the evolved materials. In friction stir-related processes, the generated heat is increased with rotational speed. The grain size measurements show that the grain size increases with increasing rotational speed and heat input. Second-phase particles through the microstructure may exert a Zener pinning effect, which can influence dislocation activity and restrict grain boundary movement—both of which are important in recrystallization and grain growth phenomena [23]. However, it seems that their effect on grain boundary movement was negligible, as the particle distribution (Figs. 2 and 3) did not vary significantly with processing parameters. An XRD and EDS analysis was conducted on the sample with the highest heat input and larger grains to investigate the possibility of any second-phase particles. Fig. 5a shows the XRD results from the processed sample at 2500 rpm, which proves the intermetallic nature of these particles. The diffraction pattern predominantly displays peaks corresponding to the aluminum phase, with a few minor peaks indicating the presence of intermetallic compounds. EDS point analysis was conducted on different particles in different regions of the sample processed with a 2500 rpm rotational speed. As indicated, EDS analysis was conducted on different particles; as the results were similar, only three results were provided. These results further confirm the presence of intermetallic compounds, including elements like Fe, Mn, Si, and Mg. Intermetallic compounds are, in fact, precipitates, constituent phases, and dispersoids with diverse chemical composition in a wide range of dimensions from the nano-to microscale. Depending on whether the constituent particles are soluble in the subsequent heat treatment process, they can be divided into two categories: insoluble constituent particles and soluble/partially soluble constituent particles. Insoluble constituent phases are formed during solidification at high temperatures and are normally not affected by subsequent heat treatments, having a minor contribution to mechanical properties. In addition, they are relatively large (>1 μm), irregularly shaped, and rather diverse in chemical composition, containing different amounts of Al, Cu, Fe, Mn, and Si and characteristically crystallizing in a variety of atomic structures. The insoluble constituent particles have a negligible effect on strength owing to the incoherent ratio of constituent particles to the matrix, and their larger size. However, soluble/partially soluble constituent particles that emerge in response to age-hardening process can greatly contribute mechanical strength in aluminum alloys [32,33]. Thermally stable constituent particles are crushed and redistributed in the weld under the stirring action of the tool during FSW, so, in principle, their volume fraction should be maintained [32]. However, some researchers [34] have noticed that the volume fraction of thermally stable constituent particles in aluminum alloys decreases; a more likely explanation is that the insoluble constituent particles are crushed or eroded, such that the particle size is less than the detection limit.

It is seen that the compounds are AlFeMgSi, AlFeMnSi, and AlMnSi particles [35,36]. Microstructural observations revealed that, from the viewpoint of particle size, they fall into two groups, i.e., micro-sized and submicron-sized, which are distinctly visible in Fig. 6. Comparing the scale bar with the size of oxide particles shows that the dimensions of the bigger particles are in the range of 1–6 μm, while the other small particles are in submicron levels, with an average dimension of about 300 nm. The stirring action of the tool bends and breaks the intermetallic compounds, which can also be observed in the microstructure of the processed sample at 2500 rpm (Fig. 2D). Layers of these intermetallic compounds are bent during stirring and fragmented into several pieces. Microstructural observations show that large second-phase particles tend to sit either on grain boundaries or, in some rare cases, inside the grains (Fig. 6). Fig. 6 also shows that the large interior particles fragment the occupied grain into several domains by developing new grain

Table 2
Experimental scheme for analyzing the influence of key FSC process parameters.

Exp ID	Rotational speed [RPM]	Consolidation Force [kN]	Processing Time [s]
Exp 1	1500	20	60
Exp 2	2000	20	60
Exp 3	2500	20	60
Exp 4	1500	10	60
Exp 5	1500	15	60
Exp 6	1500	15	90

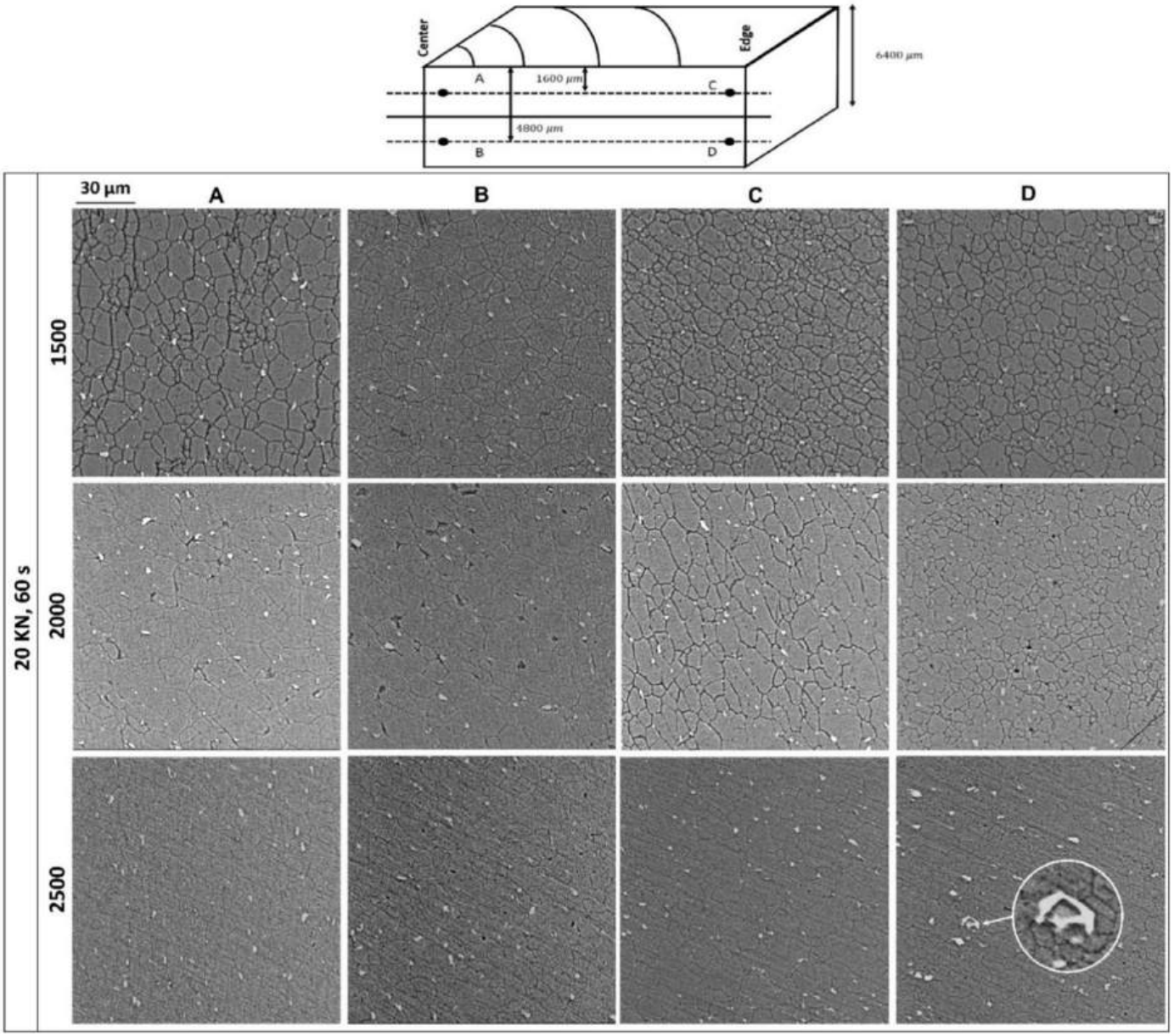

Fig. 2. Back-scattered electron images taken from the different regions of the sample processed with different rotational speeds.

boundaries. It is well established that second-phase particles can enhance the recrystallization process by increasing the stored energy in the material, thereby raising the driving force for recrystallization. It is well documented that second-phase particles can serve as effective nucleation sites for recrystallization, as depicted in Fig. 6b. On the other hand, very close particles can have a pinning effect on grain boundaries, resulting in the prevention of the recrystallization process [23]. Therefore, particles can retard or accelerate the recrystallization process, which depends on the mentioned factors. According to Humphreys et al. [23], new strain-free grains can be developed by the presence of large second-phase particles with a diameter greater than 1 μm, known as particle-stimulated nucleation (PSN). As shown in Fig. 6, the microstructural analysis indicates that larger particles facilitate recrystallization during processing by serving as nucleation sites for new grains. This process leads to the development of new domains and the fragmentation of existing grains, providing clear evidence of the particle-stimulated nucleation (PSN) mechanism. PSN has already been observed and reported in the microstructure of Al-based metal matrix composites subjected to friction stir welding/processing [37–39].

Surface oxides of the chips are one of the other important subjects that should be considered, as they remain inside the microstructure and might affect the final properties of the recycled material. Detailed EBSD scans were conducted, with a very small step size of 50 nm, on the microstructure of the sample produced with tool rotation equal to 2500 rpm, tool force equal to 20 kN, and process time equal to 60 s (Fig. 7). The corresponding phase maps show the presence of less than 0.1 percent Aluminum oxide particles, which preferably precipitated on the grain boundaries. The latter percent can explain why, due to the lower fraction of small particle size, XRD patterns cannot give any peak for the formation of these oxides. By comparing the scale bar with the dimensions of the oxides, it is evident that the oxides are nanometric in size. Since PSN is unlikely to occur when particle size falls below 1 μm, the surface oxides do not contribute to PSN-driven recrystallization. However, it has been demonstrated that the activation energy and the recrystallization critical strain decreased in the presence of Al_2O_3 nano-sized particles. Additionally, distortion zones formed by Al_2O_3 particles served as potential nucleation sites, alongside grain boundaries, for DRX. These particles facilitated the transition from LAGBs to HAGBs

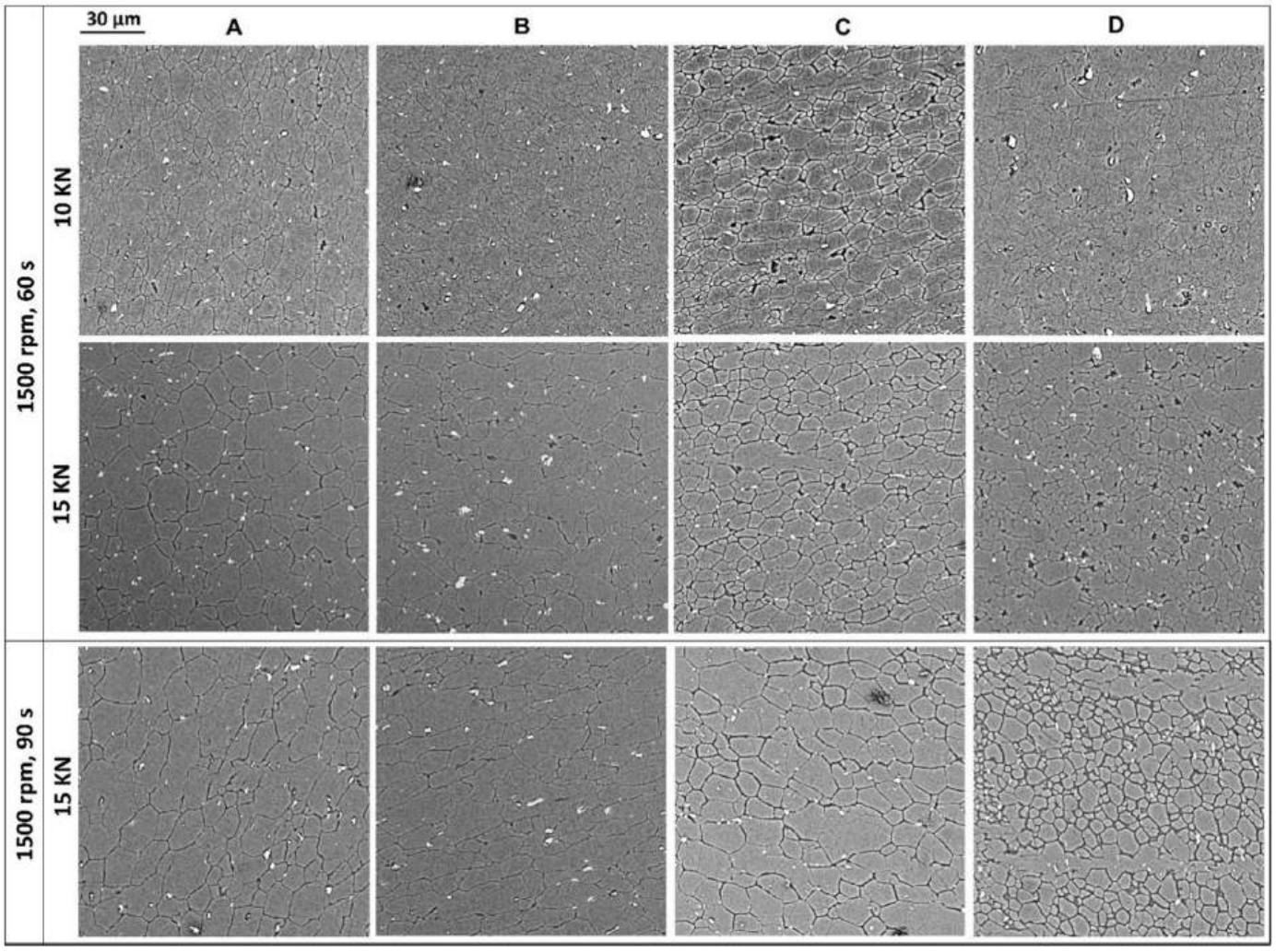

Fig. 3. Back-scattered electron images taken from the different regions of the sample obtained with different forces and processing times.

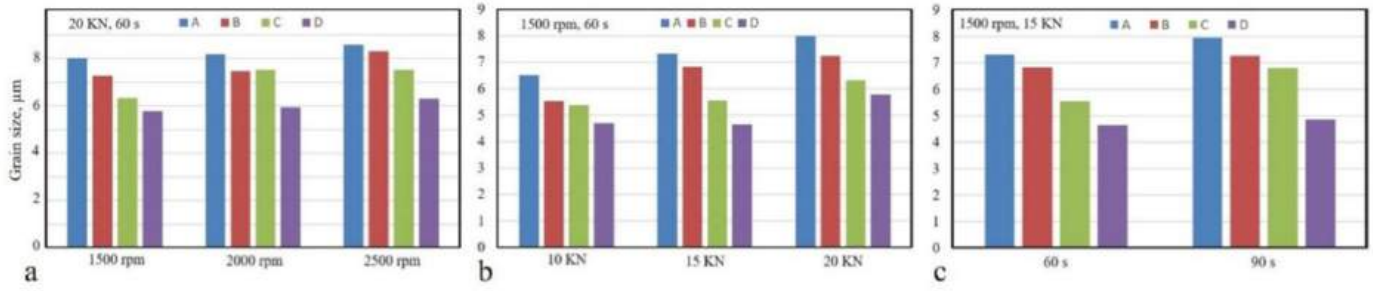

Fig. 4. Average grain size distribution through the microstructure of processed materials as a function of (a) rotational speed, (b) tool force, and (c) process time.

during high-temperature deformation, leading to a more pronounced DRX process [40].

To investigate the microstructural evolution, EBSD analysis was conducted on samples with different rotational speeds and vertical down forces. Fig. 8 presents inverse pole figure (IPF) maps with corresponding misorientation angle histograms. IPFs indicate that the concurrent application of severe plastic deformation and heat generated during the FSC process has resulted in fine recrystallized microstructures within the introduced billets. As indicated in Fig. 8, misorientation angle histograms displayed distinct peaks in the low-angle region, confirming the presence of low-angle grain boundaries (LAGBs) within the microstructure. The development of a higher LAGB fraction can be attributed to the occurrence of the dynamic recovery (DRV) process in the region. Similar behavior has also been reported in the microstructures of various alloys subjected to the friction stir welding process. [41, 42]. The DRV process involves the annihilation and rearrangement of slip dislocations, leading to the formation of low-energy dislocation structures commonly referred to as LAGBs [23]. The intensity of this phenomenon is directly related to the amount of applied strain and the dislocation density, i.e., the process is accelerated at higher strains and dislocation densities. This process leads to a steady-state condition in which the work-hardening effect, driven by dislocation generation

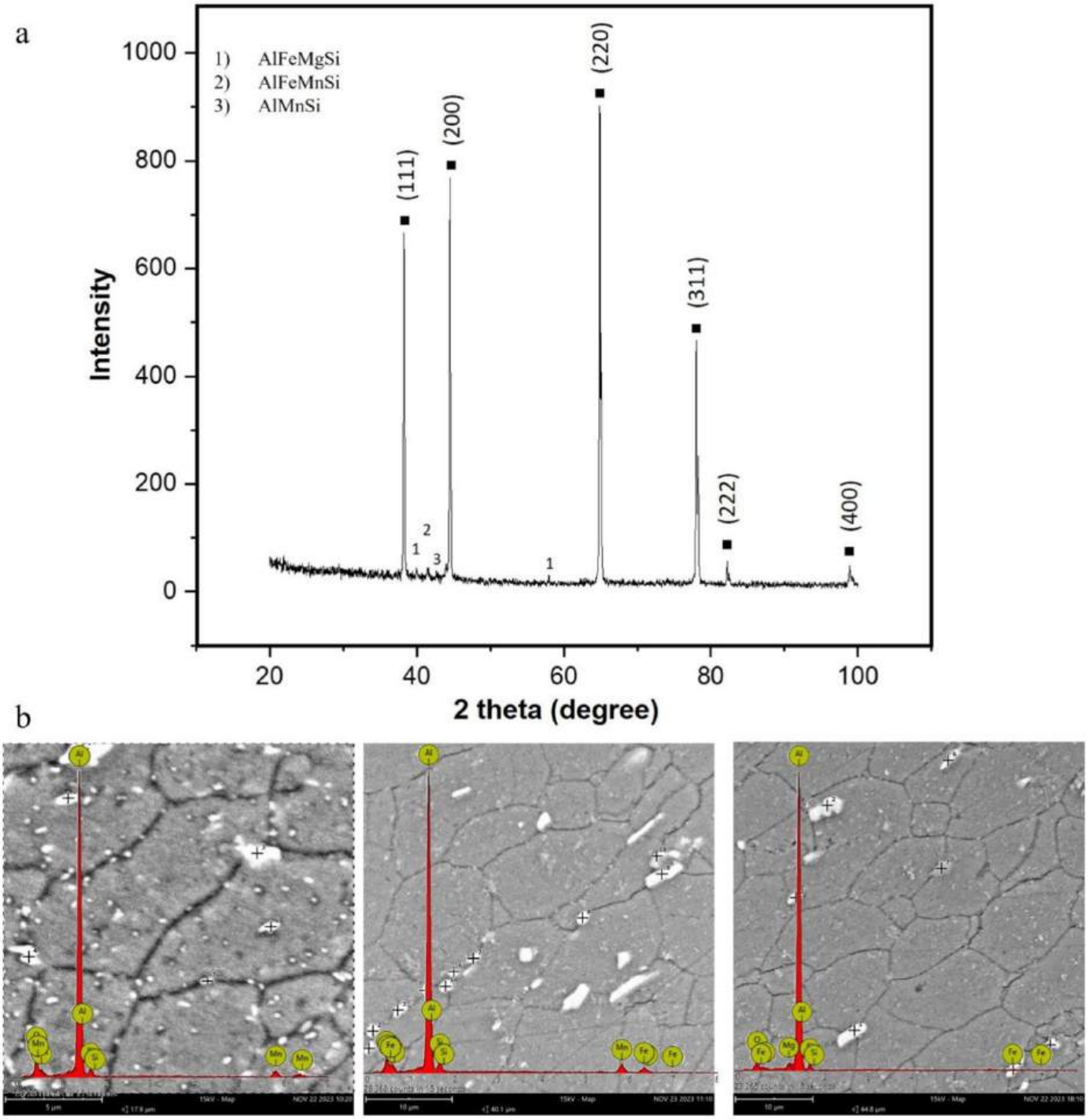

Fig. 5. Particle characterizations of the sample processed with 2500 rpm; a) XRD, and b) EDS analysis.

during deformation, is balanced by the work-softening effect resulting from dislocation annihilation and rearrangement. Dynamic recrystallization (DRX) initiates with the nucleation of new grains once a sufficient driving force is generated through the progressive accumulation of dislocations. New recrystallized grains form either continuously—through increasing misorientation angles via subgrain coalescence or rotation, a mechanism known as continuous dynamic recrystallization (CDRX)—or discontinuously, through the bulging of pre-existing grain boundaries, a process referred to as discontinuous dynamic recrystallization (DDRX). The occurrence of these recrystallization mechanisms is primarily influenced by factors such as stacking fault energy (SFE), deformation conditions, and temperature [23,41]. Additionally, the orientation map reveals the presence of equiaxed recrystallized grains throughout the microstructure. It is seen that the fraction of the LAGBs increases with increasing vertical downforce from 10 kN (Fig. 8a) to 20 kN (Fig. 8b), as the degree of deformation increases. Statistical data also reveal that there is a deformation gradient across the longitudinal cross-section of the billets. Results show that the fraction of the LAGBs increases from the bottom of the billet, where the material receives lower degrees of deformation and temperature, towards the top of the billet, where the material is in direct contact with the rotating tool and experiences higher temperature and deformation.

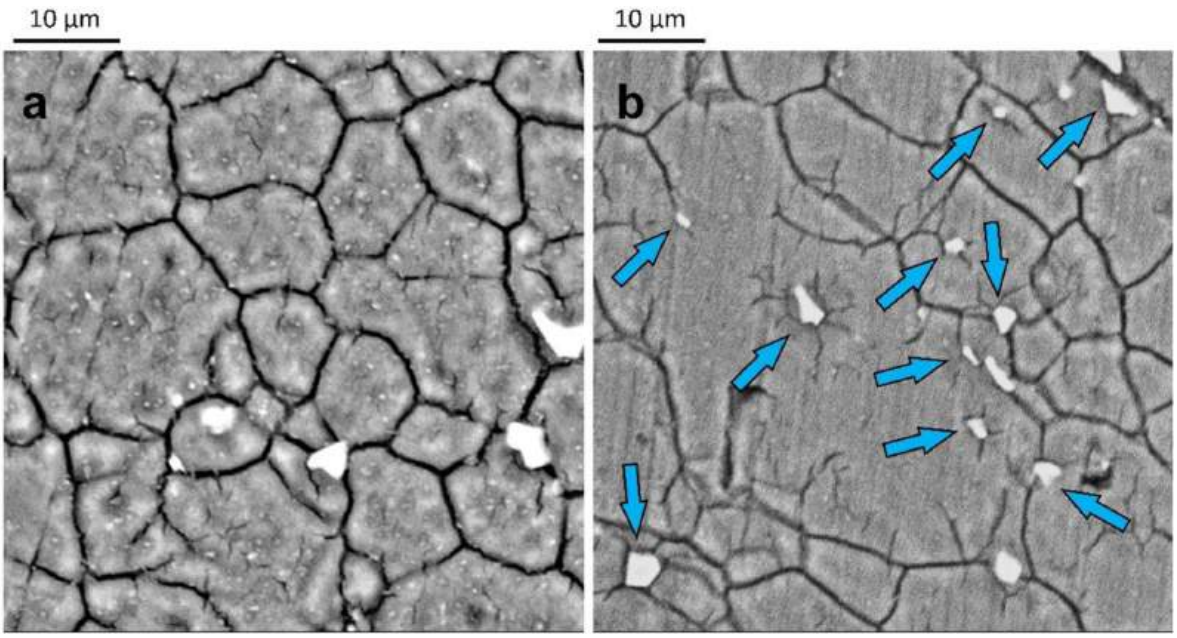

Fig. 6. BSE images obtained from the microstructure of the processed sample at 1500 rpm; a) show both micro and submicron-sized oxides through the microstructure, b) indicate oxide role in the formation and development of recrystallization process.

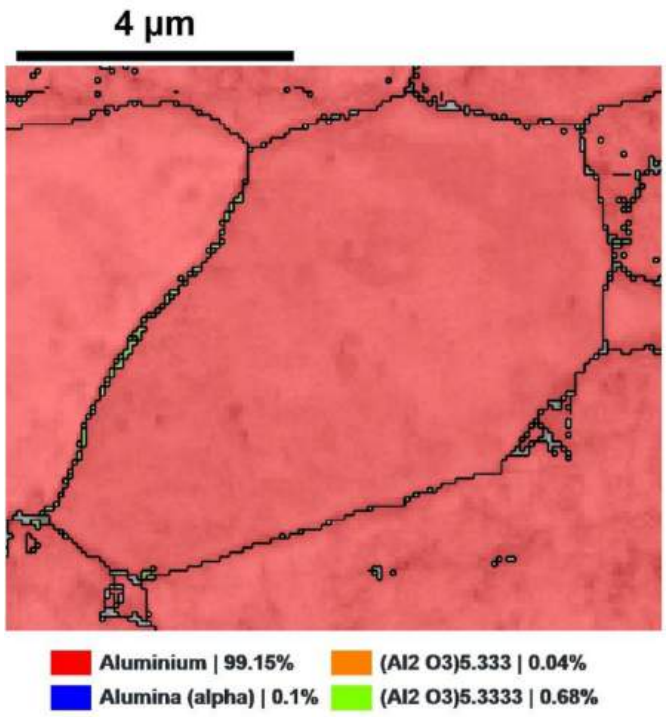

Fig. 7. Phase maps obtained from the sample processed at 2500 rpm, 20 kN, 60 s, showing the formation of Al oxides along the grain boundaries.

The presence of misorientation angles in the range of 10°–15°, along with the presence of loose or incomplete high-angle grain boundaries indicated in Fig. 9, suggests the occurrence of CDRX. This behavior has also been observed in the microstructures of austenitic, ferritic, and duplex stainless steels during the friction stir welding process [34]. CDRX usually occurs homogeneously with no recognizable nucleation and growth throughout the microstructure. Through this mechanism, LAGBs increase the associated misorientation angle by absorbing the lattice dislocations and forming HAGBs. CDRX is a single-step recrystallization mechanism that takes place in all materials at temperatures below 0.5 Tm, and also occurs in materials with medium to high stacking fault energy (SFE) when the temperature exceeds 0.5 Tm [42]. Several studies have reported similar CDRX behavior in other aluminum alloys under comparable thermomechanical conditions, especially during severe plastic deformation or friction-based processes like friction stir welding and consolidation. For instance, alloys such as AA1421 [43] and AA2195 [44,45], AA6061-T6 [46], AA5251 [47], AA5052 [48] have shown microstructural features consistent with CDRX, including equiaxed grains, progressive misorientation development, and the absence of distinct nucleation sites.

Since the FSC process imposes high vertical pressure with concurrent torsional straining, it follows the fundamentals of the high-pressure torsion (HPT) process. Like the HPT process, the FSC process induces a greater degree of shear deformation in the material through the mechanical action of the rotating tool. During plastic deformation, the shape and orientation of individual grains in a polycrystalline material tend to change in response to the direction of the applied stresses. Therefore, the grain rotation occurs in a preferred orientation known as texture. This kind of modification takes place by the easy slip planes, which tend to gradually reorient themselves parallel to the shear plane during deformation. Torsion textures can be described as {hkl}<uvw>, where {hkl} is parallel to the shear plane and <uvw> is parallel to the shear direction [49]. It is to be mentioned that the common FCC fibers are {111}//SP and <110>//SD, which follow from the active slip plane and slip direction [50]. Fig. 10 shows the {111} and {110} pole figures derived from the microstructure of samples processed at 1500 rpm under 10 kN and 20 kN, as well as at 2500 rpm under 20 kN, obtained from the longitudinal cross-section of the billet, which is parallel to the compression direction (CD). It should be mentioned that the introduced texture components can be described in different spaces linked to the sample coordinate system. The obtained pole figures differ with respect to the plane measurements for the SD-RD, SD-CD, and CD-RD planes, where SD represents the shear direction, RD is the radial direction, and CD is the compression direction. Here, based on the measurements from the longitudinal cross-section, the resulting textures have been characterized by CD-SD pole figures, which define the shear texture components [51].

The shear plane is parallel to the surface of the rotating tool, and the

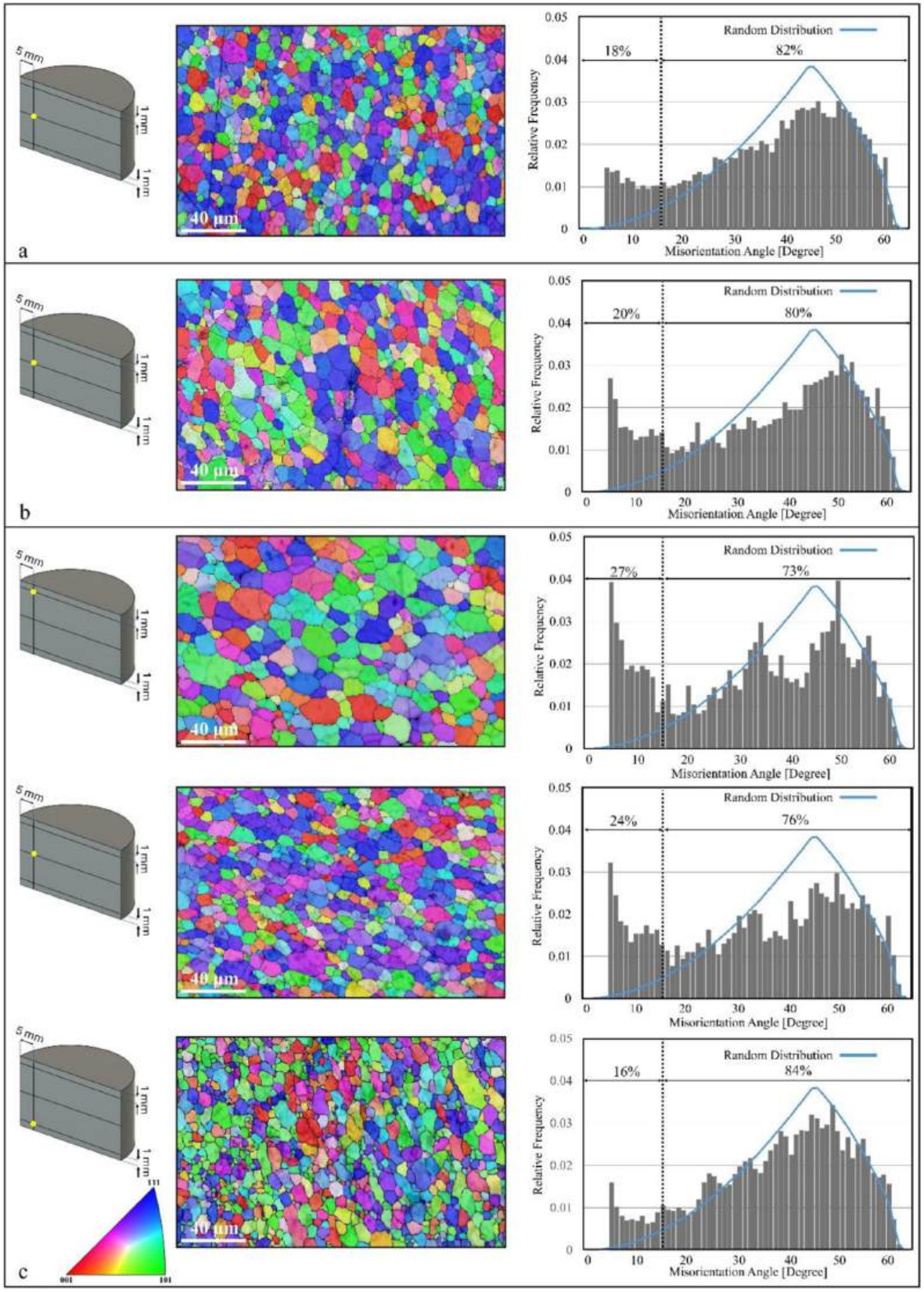

Fig. 8. EBSD data showing orientation maps and corresponding misorientation angle histograms, obtained from the longitudinal cross-section of the produced billets at; a) 1500 rpm, 10 kN, 60 s, b) 1500 rpm, 20 kN, 60s, and c) 2500 rpm, 20 kN, 60 s.

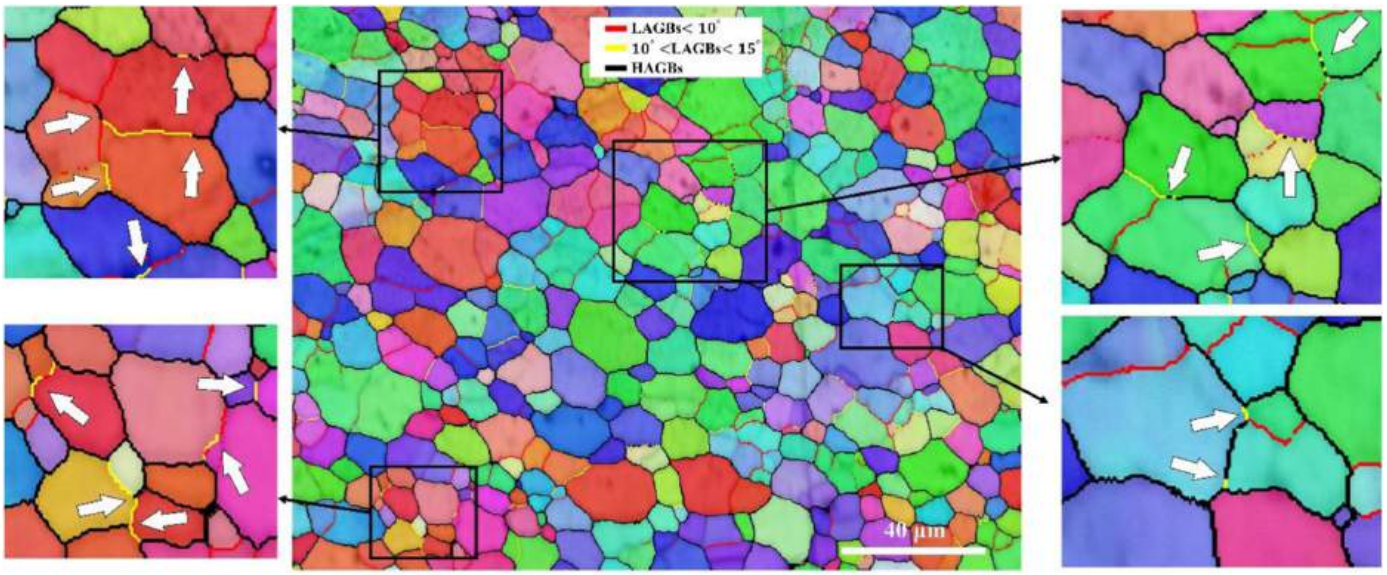

Fig. 9. Inverse pole figure map superimposed with grain boundary map obtained from the microstructure of the billet processed with a 2500 rpm rotational speed.

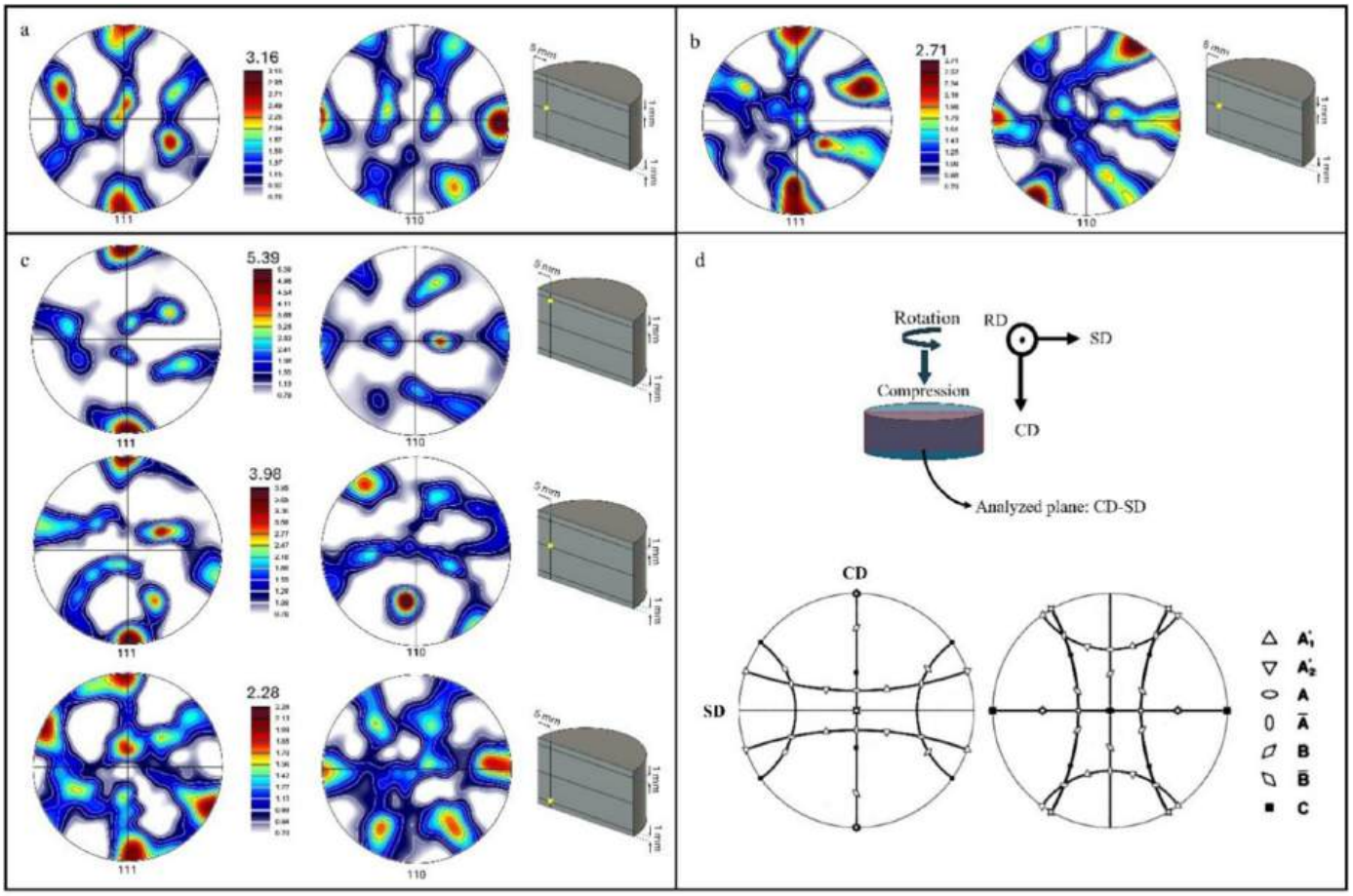

Fig. 10. 111 and 110 pole figures obtained from different samples; a) 1500 rpm and 10 kN, b) 1500 rpm and 20 kN, c) 2500 rpm and 20 kN, and d) schematics showing FSC principles and positions of the ideal shear texture components on the CD-SD planes for FCC structured materials [51,52,53].

shear direction lies on the shear plane, as confirmed by previous numerical simulations [54], and the HPT process [55–57]. As the EBSD scans have been conducted on longitudinal cross-sections, pole figures and texture data are better shown CD-SD frame of reference, like what is reported for HPT samples [51]. But regarding the thickness of the FSC samples, microscopic deformation coordinates (the shear plane Normal – the shear direction (SPN-SD)), can build up different angles with the macroscopic deformation coordinates (CD-SD-RD) as the distance from the shoulder increases, owing to the strain gradient across the billet axis. Under the shoulder, the shear plane is parallel with the rotating surface

of the tool; therefore, the shear plane normal (SPN) is parallel with the compression direction (CD), but running towards the bottom of the billet, similar to FS welded materials shear plane loses its parallel relationship with the surface of the rotating tool [52]. Comparing the ideal texture components in Fig. 10d with the experimental results in Fig. 10a–c revealed that the FSC process induced simple shear texture components within the microstructures. The same behavior has been observed in the microstructure of processed nickel and copper with high-pressure torsion [55–57].

The orientation distribution function (ODF) has been calculated to characterize the distribution of the developed textures more accurately. Accordingly, Fig. 11 shows the $\varphi_2 = 0$ and $\varphi_2 = 45$ sections of corresponding ODFs. A comparison between these ODF sections and the ideal ODF sections for FCC materials subjected to simple shear deformation (Fig. 11d) confirms the formation of shear textural components through the microstructure of the evolved material. ODF sections taken along the billet axis, from top to bottom, reveal a texture gradient that decreases toward the bottom. This trend occurred because the material near the rotating tool experienced a higher degree of deformation and elevated temperature. It is also observed that the C component tends to form as the rotation speed increases from 1500 rpm to 2500 rpm. Furthermore, the ODF sections reveal the presence of cube texture components, marked by red triangles in both $\varphi_2 = 0$ and $\varphi_2 = 45$ sections. This component is more likely the "Oblique Cube" component, which represents a rotated variant of the classic Cube $\{001\}\langle100\rangle$ recrystallization texture, shifted around the radial axis from its ideal crystallographic orientation. With progressive deformation, Cube-oriented grains experience a rotation about the radial direction, resulting in the formation of the Oblique Cube component [51]. In pure nickel subjected to high-pressure torsion (HPT), increasing the deformation temperature alters the microstructure, resulting in the disappearance of the C component and the emergence of a new Oblique Cube component [51, 58]. Cube texture has also been reported from the microstructure of commercial purity aluminum subjected to the HPT process [59].

Fig. 12 illustrates the microhardness distribution across the axial cross-section of the billet processed at a rotational speed of 2500 rpm via friction stir consolidation. The mapping reveals a distinct hardness gradient, with higher values near the top surface—closer to the rotating tool—and progressively lower values toward the bottom. This non-uniformity stems from the inherent nature of the FSC process, where the material near the tool experiences intense plastic deformation and elevated temperatures, leading to greater stored energy and dynamic recrystallization. In contrast, regions farther from the tool undergo less severe thermomechanical exposure, resulting in reduced substructural refinement. The elevated hardness near the surface is consistent with previous findings that attribute such increases to the formation of low-angle grain boundaries (LAGBs) and a high density of dislocations generated during straining. These substructures act as effective barriers to dislocation motion, thereby enhancing hardness. Notably, the gradient suggests that substructural features—rather than grain size alone—play a dominant role in determining local hardness [60,61]. Moreover, the gradient reflects the anisotropic nature of energy input during FSC. The top regions, being in direct contact with the rotating tool, absorb more frictional heat and mechanical work, promoting dynamic recovery and sub-grain formation. These microstructural changes contribute to localized strengthening. Conversely, the bottom regions, shielded from direct tool interaction, retain a more coarse and less deformed structure, resulting in lower hardness [62]. The distribution of hardness can also be attributed to the intensity of the developed textures. Studies have shown that a pronounced {111} texture component significantly influences material hardness, providing a stronger hardening effect compared to other crystallographic orientations in face-centered cubic (FCC) materials [63].

It is also to be mentioned that numerous investigations on the FSW of

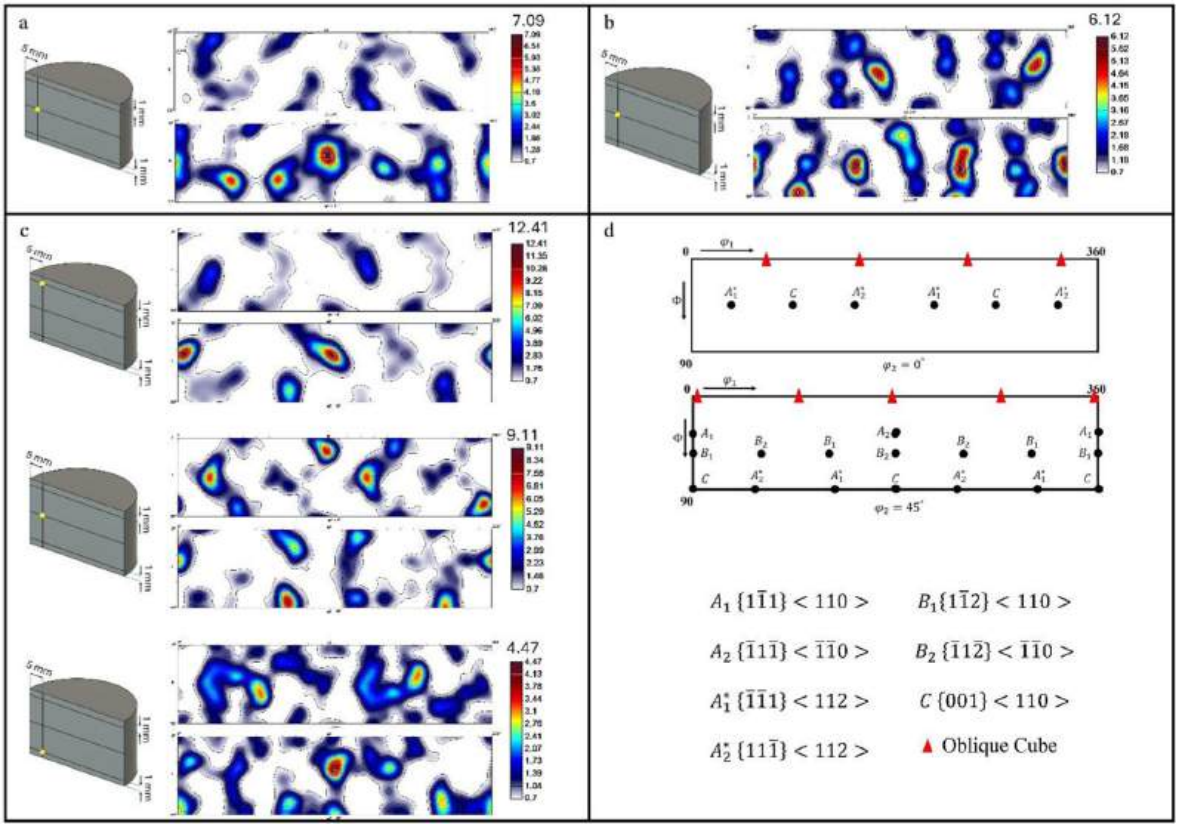

Fig. 11. a) ODF sections obtained from different samples; a) 1500 rpm and 10 kN, b) 1500 rpm and 20 kN, c) 2500 rpm and 20 kN, and b) Locations of the ideal components of simple shear texture in the fcc metals at $\varphi_2 = 0°$ and $\varphi_2 = 45°$ from Ref. [51].

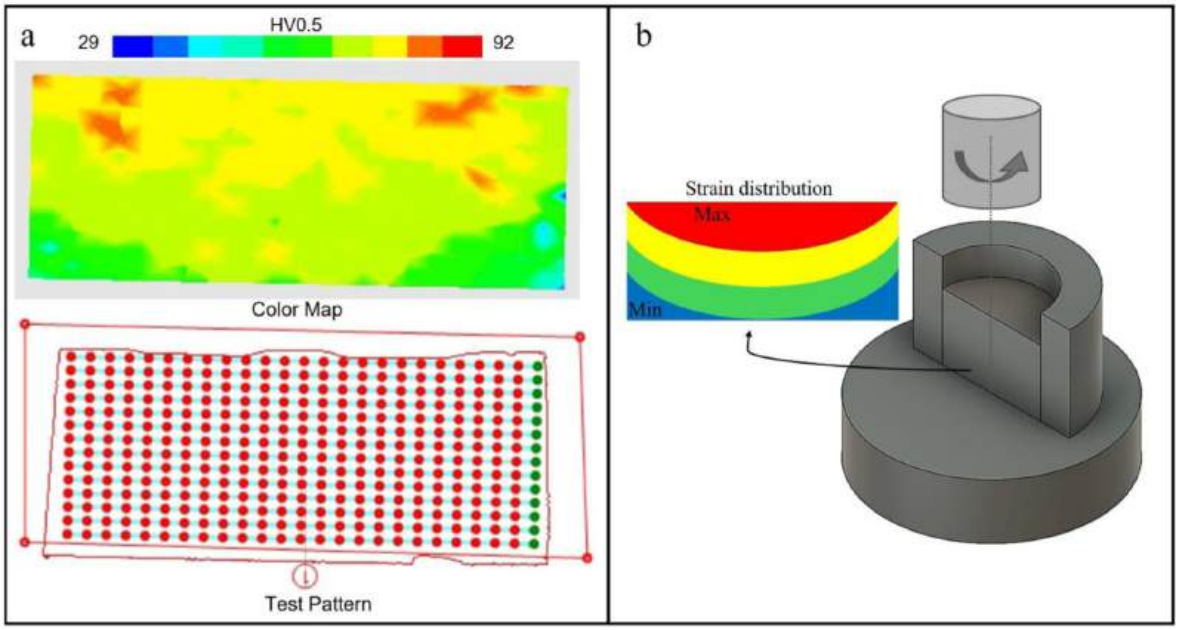

Fig. 12. a) Two-dimensional color-coded contour map showing the Vickers microhardness distributions across the billet axial cross-section, b) a schematic of the strain state through the longitudinal cross-section.

heat-treatable aluminum alloys have shown that second-phase particles containing heavy elements like Fe, exhibit high thermal stability and do not dissolve under the combined thermal and mechanical conditions of the FSW process and are uniformly distributed through the microstructure of the evolved material. Although they do not directly contribute to the strengthening of the joint, dispersoids act as effective nucleation sites for precipitate formation, thereby facilitating dispersion strengthening in aluminum alloy [32].

4. Conclusions

Friction stir consolidation (FSC) of AA 6082 aluminum chips was investigated in the present study. Different specimens were produced with varying tool rotation, tool force, and processing time. The key findings of this study can be summarized as follows:

1. Fine equiaxed grain structures were developed through the microstructure of the processed samples. Different processing parameters resulted in different grain structures. Parameters associated with higher heat input, i.e. higher tool rotation, tool force, and/or processing time, resulted in coarse grains while finer grains were observed when low heat input parameters were adopted.
2. In each sample, different microstructural regions showed different grain sizes owing to the temperature and strain rate gradient. Coarser grains were obtained in the center of the billet near the shoulder, where the material experienced the highest heat input, and the smallest grains were developed in the bottom part of the billet near the surface, where the material experienced the smallest amount of heat and applied strain.
3. The intermetallic nature of the bright particles was confirmed using the XRD pattern. The stirring action of the rotating tool broke down the large intermetallic compounds and created micro and Nano-sized second-phase particles.
4. The grain boundary map revealed the presence of incomplete high-angle grain boundaries (HAGBs) connected to low-angle grain boundaries (LAGBs), which suggest the occurrence of continuous dynamic recrystallization (CDRX).
5. Texture analysis showed that the FSC process developed simple shear texture components through the microstructure of the evolved material.
6. The hardness value increased with the fraction of LAGBs and texture intensity.

Declaration of competing interest

The authors declare that they have no known competing financial interests or personal relationships that could have appeared to influence the work reported in this paper.

Acknowledgments

This study was carried out within the research activities of the project “Finalizing processes for multimaterial based Functionally Graded billets and wires obtained through solid state recycling operations of aluminum alloy chips – FULL RECYCLE” (2022X5RPSM PRIN 2022), financed by the European Community – Next Generation EU. This manuscript reflects only the Authors' views and opinions, neither the European Union nor the European Commission can be considered responsible for them.

References

[1] Wan B, Chen W, Lu T, Liu F, Jiang Z, Mao M, et al. Review of solid state recycling of aluminum chips. Resour Conserv Recycl 2017;125:37–47.
[2] Güley V, Güzel A, Jäger A, BenKhalifa N, Tekkaya AE, Misiolek WZ, et al. Effect of die design on the welding quality during solid state recycling of AA6060 chips by hot extrusion. Mater Sci Eng, A 2013;574:163–75.
[3] Mohammed RH, Shahab AF, Rezaei AF. Effect of ECAP process on mechanical properties and microstructure of AA-6061 recycled chips. Eng Technol J 2023;41 (7).
[4] Al-Alimi S, Lajis MA, Shamsudin S, Yusuf NK, Chan BL, Hissein DD, et al. Hot extrusion followed by a hot ECAP consolidation combined technique in the production of boron carbide (B4C) reinforced with aluminium chips (AA6061) composite. Mater Technol 2021;55(3):347–54.
[5] Selmy AI, Abd El Aal MI, El-Gohry AM, Taha MA. Solid-state recycling of aluminum alloy (AA-6061) chips via hot extrusion followed by equal channel angular pressing. ECAP) 2016;21:33–42.
[6] Taha MA, Abbas AT, Benyahia F, Alharbi HF, Guitian B, Novoa XR, et al. Enhanced corrosion resistance of recycled aluminum alloy 6061 chips using hot extrusion followed by ECAP. J Chem 2019:1–8.

[7] Abd El Aal MI. Recycling of Al chips and Al chips composites using high-pressure torsion. Mater Res Express 2021;8:056514.
[8] Shi Q, Tse YY, Higginson RL. Effects of processing parameters on relative density, microhardness and microstructure of recycled Ti–6Al–4V from machining chips produced by equal channel angular pressing. Mater Sci Eng, A 2016;651:248–58.
[9] Haase M, Ben Khalifaa N, Tekkaya AE, Misiolek WZ. Improving mechanical properties of chip-based aluminum extrudates by integrated extrusion and equal channel angular pressing (iECAP). Mater Sci Eng 2012;539:194–204.
[10] Whalen S, Taysom BS, Overman N, Reza-E-Rabby M, Qiao Y, Richter T, et al. Porthole die extrusion of aluminum 6063 industrial scrap by shear assisted processing and extrusion. Manufacturing Letters 2023;36:52–6.
[11] Kolpak F, Schulze A, Dahnke C, Tekkaya AE. Predicting weld-quality in direct hot extrusion of aluminium chips. J Mater Process Technol 2019;274:116294.
[12] Chiba R, Yoshimura M. Solid-state recycling of aluminium alloy swarf into c-channel by hot extrusion. J Manuf Process 2015;17:1–8.
[13] Ying T, Zheng MY, Hu XS, Wu K. Recycling of AZ91 Mg alloy through consolidation of machined chips by extrusion and ECAP. Trans Nonferrous Metals Soc China 2010;20:s604–7.
[14] Pei Y, Ma H, Yuan M, Teng B. Solid state recycling of Mg–Gd–Y–Zn–Zr alloy chips by isothermal sintering and equal channel angular pressing. J Magnesium Alloys 2024;12(7):2725–40.
[15] Ingarao G, Amato M, Latif A, La Rosa AD, Di Lorenzo R, Fratini L, et al. Life cycle assessment of aluminum alloys chips recycling through single and multi-step Friction Stir Consolidation processes. J Manuf Syst 2023;68:651–9.
[16] Li X, Baffari D, Reynolds AP. Friction stir consolidation of aluminum machining chips. Int J Adv Manuf Technol 2018;94:2031–42.
[17] Buffa G, Baffari D, Ingarao G, Fratini L, et al. Uncovering technological and environmental potentials of aluminum alloy scraps recycling through friction stir consolidation. International Journal of Precision Engineering and Manufacturing-Green Technology 2020;7:955–64.
[18] Latif A, Ingarao G, Fratini L. Multi-material based functionally graded billets manufacturing through friction stir consolidation of aluminium alloys chips. CIRP Ann - Manuf Technol 2022;71:261–4.
[19] Latif A, Ingarao G, Gucciardi M, Fratini L. A novel approach to enhance mechanical properties during recycling of aluminum alloy scrap through friction stir consolidation. Int J Adv Manuf Technol 2022;119:1989–2005.
[20] Abdi Behnagh R, Fathi F, Yeganeh M, Paydar M, Agha Mohammad M, Liao Y. Production of seamless tube from aluminum machining chips via double-step friction stir consolidation. Int J Adv Manuf Technol 2019;104:4769–77.
[21] Abebe SK, Beri H, Sinha DK, Rajhi AA, Hossain N, Duhduh AA, et al. Wear behavior of AZ61 matrix hybrid composite fabricated via friction stir consolidation: a combined RSM box–behnken and genetic algorithm optimization. J Compos Sci 2023;7:275.
[22] Latif A, Ingarao G, Buffa G, Fratini L. Forgeability characterization of multi-material based functionally graded materials manufactured through friction stir consolidation. In: The 19th international conference on metal forming, 1270; 2022, 012096.
[23] Humphreys FJ, Hatherly M. Recrystallization and related annealing phenomena. second ed. Amsterdam: Elsevier; 2004.
[24] Wagiman A, Mustapa MS, Asmawi R, Shamsudin S, Lajis MA, Mutoh Y. A review on direct hot extrusion technique in recycling of aluminium chips. Int J Adv Manuf Technol 2020;106:641–53.
[25] Laurent-Brocq M, Lilensten L, Pinot C, Schulze A, Duchaussoy A, Bourgon J, et al. Solid state recycling of aluminium chips: multi-technique characterization and analysis of oxidation. Materialia 2023;31:1018.
[26] Rolseth A, Carlson M, Ghassemali E, Pérez Caro L, Jarfors AEW. Impact of functional integration and electrification on aluminium scrap in the automotive sector: a review, 205; 2024, 107532.
[27] Beausir B, Fundenberger JJ. Analysis tools for electron and X-ray diffraction. Université de Lorraine - Metz; 2017 [Internet], http://www.atex-software.eu.
[28] Hajizadeh M, Emami S, Saeid T. Influence of welding speed on microstructure formation in friction-stir-welded 304 austenitic stainless steels. Int J Miner Metall Mater 2020;27(11):1517–27.
[29] Taysom BS, Overman N, Olszta M, Reza-E-Rabby M, Skszek T, DiCiano M, et al. Shear assisted processing and extrusion of enhanced strength aluminum alloy tubing. Int J Mach Tool Manufact 2021;169:103798.
[30] Whalen S, Olszta M, Reza-E-Rabby M, Roosendaal T, Wang T, Herling D, et al. High speed manufacturing of aluminum alloy 7075 tubing by Shear assisted processing and extrusion (ShAPE). J Manuf Process 2021;71:699–710.
[31] Kalsar R, Ma X, Darsell J, Zhang D, Kappagantula K, Herling DR, et al. Microstructure evolution, enhanced aging kinetics, and mechanical properties of AA7075 alloy after friction extrusion. Mater Sci Eng, A 2022;833:142575.
[32] Wang K, Naumov A, Panchenko E, Panchenko O. A review on friction stir welding of high-strength Al-Zn-Mg alloy: insights on second-phase particles. Materials 2024;17(20):5107.
[33] Kosari A, Tichelaar F, Visser P, Zandbergen H, Terryn H, Mol JMC. Dealloying-driven local corrosion by intermetallic constituent particles and dispersoids in aerospace aluminium alloys. Corros Sci 2020;177:108947.
[34] Gallais C, Simar A, Fabregue D, Denquin A, Lapasset G, De meester B, et al. Multiscale analysis of the strength and ductility of AA 6056 aluminum friction stir welds. Metall Mater Trans 2007;38:964–81.
[35] Wang J, Mil Z, Jiang H, Wang R. Texture-governed electrochemical corrosion behavior of AA 6082 alloy. J Mater Sci 2019;54:6608–23.
[36] Kumar N, Goel S, Jayaganthan R, Brokmeier HG. Effect of solution treatment on mechanical and corrosion behaviors of 6082-T6 Al alloy. Metallogr Microstruct Anal 2015;4:411–22.
[37] Sarkari Khorrami M, Kazeminezhad M, Kokabi AH. Influence of stored strain on fabricating of Al/SiC nanocomposite by friction stir processing. Metall Mater Trans 2015;46:2021–34.
[38] Guo JF, Liu J, Sun CN, Maleksaeedi S, Bi G, Tan MJ, et al. Effects of nano-Al_2O_3 particle addition on grain structure evolution and mechanical behaviour of friction-stir-processed Al. Mater Sci Eng 2014;602:143–9.
[39] Moradi MM, Jamshidi Aval H, Jamaati R, Amirkhanlou S, Ji S. Effect of SiC nanoparticles on the microstructure and texture of friction stir welded AA2024/AA6061. Mater Char 2019;152:169–79.
[40] Liu W, Liu F, Xie G, Zhao F, Liu X. Effect of nano-scaled Al2O3 particles on dynamic recrystallization behavior and microstructure evolution of pure copper in hot deformation. Mater Sci Eng 2024;914:147123.
[41] Baradarani F, Emami S, Mostafapour A, Khan MD F. Influence of ultrasonic vibration on the microstructure and texture evolution of AZ91 magnesium alloy during ultrasonic-assisted friction stir welding. Weld World.
[42] Heidarzadeh A, Mironov S, Kaibyshev R, Çam G, Simar A, Gerlich A, et al. Friction stir welding/processing of metals and alloys: a comprehensive review on microstructural evolution. Prog Mater Sci 2021;117:100752.
[43] Kaibyshev R, Shipilova K, Musin F, Motohashi Y. Continuous dynamic recrystallization in an Al–Li–Mg–Sc alloy during equal-channel angular extrusion. Mater Sci Eng 2005;396(1–2):341–51.
[44] Fonda RW, Bingert JF, Colligan KJ. Development of grain structure during friction stir welding. Scr Mater 2004;51(3):243–8.
[45] Fonda RW, Bingert JF. Precipitation and grain refinement in a 2195 Al friction stir weld. Metall Mater Trans 2006;37:3593–604.
[46] Liu G, Murr LE, Niou CS, McClure JC, Vega FR. Microstructural aspects of the friction-stir welding of 6061-T6 aluminum. Scr Mater 1997;37(3):355–61.
[47] Etter AL, Baudin T, Fredj N, Penelle R. Recrystallization mechanisms in 5251 H14 and 5251 O aluminum friction stir welds. Mater Sci Eng 2007;445–446:94–9.
[48] Khodabakhshi F, Simchi A, Kokabi AH, Gerlich AP, Nosko M. Effects of stored strain energy on restoration mechanisms and texture components in an aluminum–magnesium alloy prepared by friction stir processing. Mater Sci Eng A 2015;642:204–14.
[49] Sonkusare R, Biswas K, Al-Hamdany N, Brokmeier HG, Kalsar R, Schell N, Gurao NP. A critical evaluation of microstructure-texture-mechanical behavior heterogeneity in high pressure torsion processed CoCuFeMnNi high entropy alloy. Mater Sci Eng, A 2020;782:139187.
[50] Suwas S, Ray RK. Crystallographic texture of materials. first ed. London: Springer; 2014.
[51] Azzeddine H, Bradai D, Baudin T, Langdon TG. Texture evolution in high-pressure torsion processing. Prog Mater Sci 2022;125:100886.
[52] Emami S, Saeid T, Azari Khosroshahi R. Microstructural evolution of friction stir welded SAF 2205 duplex stainless steel. J Alloys Compd 2018;739:678–89.
[53] Kesharwani R, Jha KK, Imam M, Sarkar C, Barsoum I. Comparison of microstructural, texture and mechanical properties of SiC and Zn particle reinforced FSW 6061-T6 aluminum alloy. J Mater Res Technol 2023;26:3301–21.
[54] Latif A, Puleo R, Ingarao G, Micari F, Fratini L. Material flow analysis in friction stir consolidation during recycling aluminum alloy chips. Materials Research Proceedings 2024;44:158–66.
[55] Korznikova EA, Mironov SY, Korznikov AV, Zhilyaev AP, Langdon TG. Microstructural evolution and electro-resistivity in HPT nickel. Mater Sci Eng, A 2012;556:437–45.
[56] Wei P, Lu C, Tieu K, Su L, Deng G, Huang W. A study on the texture evolution mechanism of nickel single crystal deformed by high pressure torsion. Mater Sci Eng, A 2017;684:239–48.
[57] Li J, Xu J, Wang CT, Shan D, Guo B, Langdon TG. Microstructural evolution and micro-compression in high-purity copper processed by high-pressure torsion. Adv Eng Mater 2016;18(2):241–50.
[58] Ghosh P, Renk O, Pippan R. Microtexture analysis of restoration mechanisms during high pressure torsion of pure nickel. Mater Sci Eng, A 2017;684:101–9 (For ODFs, Cube texture).
[59] Liu Y, Lu C, Wang H, Tieu AK, Liu B. Microstructure evolution, lattice rotation retardation and grain orientation fragmentation in commercial purity aluminium deformed by high pressure torsion. J Mater Res Technol 2020;9:6642–54 (For ODFs, cube texture).
[60] Qin W, Ren F, Doerner RP, Wei G, Lv Y, Chang S, et al. Nanochannel structures in W enhance radiation tolerance. Acta Mater 2018;153:147–55.
[61] Jiang H, Gong Q, Peterlechner M, Daum L, Rösner H, Wilde G. Hardness and microstructural evolution of CoCrFeNi high-entropy alloys during severe plastic deformation. Mater Sci Eng, A 2024;908:146758.
[62] Puleo R, Ingarao G, Fratini L. Friction stir consolidation of aluminium chips: a new approach to overcome the inhomogeneous properties of the consolidated billet. Materials Research Proceedings 2025;54:2447–54.
[63] Nagy P, Rohbeck N, Roussely G, Sortais P, Lábár JL, GubiczaJ, et al. Processing and characterization of a multibeam sputtered nanocrystalline CoCrFeNi high-entropy alloy film. Surf Coating Technol 2020;386:125465.